A primitive equation barotropic instability study of the monsoon onset vortex, 1979

By S. K. MISHRA, M. D. PATWARDHAN and L. GEORGE
Indian Institute of Tropical Meteorology, Pune-411005, India

SUMMARY

A primitive equation barotropic stability analysis of the 700 mb zonal wind profile over the Arabian Sea was performed for each day between 10 and 14 June 1979, during the onset phase of the monsoon. The flow was found to become progressively more unstable with the passage of time. The most unstable inviscid primitive equation mode has an e-folding time of 3·1 days, a wavelength of 3500 km and a westward phase speed of $1·9 \, \mathrm{m \, s^{-1}}$.

The non-geostrophic effect reduces the growth rate and changes the structure of the unstable mode significantly. It is noticed that when the normalized unstable mode is superposed on the basic state, the total field is closer to the observations. Momentum transports by the primitive equation mode and by the quasi-geostrophic approximation are in opposite directions in equatorial regions. The energetics of the primitive equation unstable mode are computed and the physical processes responsible for the westward propagation of the wave are identified.

1. INTRODUCTION

It has been inferred from the surface synoptic climatology during the onset of the south-west monsoon over the west coast of India, that the formation of cyclonic systems at the leading edge of the advancing monsoon current is not uncommon (Ananthakrishnan *et al.* 1968; Mukherjee and Paul 1980). In some years, the onset and advance of the monsoon are associated with the appearance of cyclonic vortices at 700 mb. Using the MONEX-1979 (GARP Summer Monsoon Experiment) data set, Krishnamurti *et al.* (1981) have depicted the evolution of the cyclonic vortex (onset vortex) at 850 mb over the south-east Arabian Sea during the period 12 to 20 June in association with the monsoon onset over India.

The three-dimensional structure of the onset vortex during MONEX-1979 has been studied by Huj (1980) and others. Huj concluded that the onset vortex first appeared on 12 June at 700 mb near 9°N as a closed cyclonic circulation. The strongest cyclonic circulation of the fully developed vortex is found in the 700–500 mb layer. The scale of the onset vortex in the zonal direction (zonal wavelength) is around 3000 km.

A few studies have been made in order to understand the dynamical processes involved in the initial formation and subsequent intensification of the onset vortex by using the MONEX data set. The results of a non-divergent barotropic stability analysis (Krishnamurti *et al.* 1981) and of a combined barotropic–baroclinic stability analysis, based on a two-layer balance model, of zonal wind profiles over the Arabian Sea before and during the onset vortex (Mak and Kao 1982) have indicated that barotropic instability may be responsible for the initiation of the onset vortex. It has also been noticed by them that vertical shear does not contribute to the growth of model disturbances but it has a significant influence on the structure. However, the flow around 10°N over the Arabian Sea is characterized by a strong vertical shear. Thus, we cannot rule out the possible existence of baroclinic instability in the onset vortex. In this connection it may be noted that recent studies (Mak 1975; Borde and Mak 1978; Mishra and Salvekar 1980) have shown that to realize the baroclinic instability of the monsoon flow, quite a large number of levels are required. Since a high resolution primitive equation barotropic–baroclinic numerical model requires very large computer memory and time,

we have not attempted to perform the combined barotropic–baroclinic stability analysis for the onset vortex.

Since the onset vortex extends up to the equator, it is expected that non-geostrophic effects are not insignificant, and we intend to investigate in this study the non-geostrophic barotropic instability characteristics of westerly flow over the Arabian Sea during the onset period by using the linear primitive equation barotropic model.

2. DESCRIPTION OF THE MODEL AND BOUNDARY CONDITIONS

In order tò incorporate the effect of vertical stratification of the atmosphere, a gravitationally stable two-layer system of homogeneous, incompressible and non-mixing fluids in hydrostatic balance is considered. The top layer of the system is infinitely deep and motionless. The infinitesimally small perturbation motion superposed on the basic state zonal wind, $\bar{u}(y)$, is governed by the linear momentum and continuity (mass conservation) equations:

$$u_t + \bar{u}u_x + v\bar{u}_y - fv + Ku = -g^*h_x \tag{1a}$$

$$v_t + \bar{u}v_x + fu + Kv = -g^*h_y \tag{1b}$$

$$(H_0 + \bar{h})(u_x + v_y) + (h_t + \bar{u}h_x + v\bar{h}_y) = 0 \tag{1c}$$

where

$$f\bar{u} = -g^*\bar{h}_y \qquad f = f_0 + \beta y \qquad g^* = g(\theta_2 - \theta_1)/\theta_2. \tag{2}$$

The overbar symbol denotes basic state quantities. u, v and h are the eastward and northward components of the perturbation velocity, and the perturbation deviation of the interface, respectively. g^* is the reduced gravity; θ_1 and θ_2 ($\theta_1 < \theta_2$) are mean potential temperatures of lower and upper layers, respectively; β is the Rossby parameter; K is the Rayleigh friction coefficient; and H_0 is the constant depth of the lower layer in the absence of any motion. Subscripts x, y and t denote differentiation. The vertical stratification effect on the motions in the lower layer is incorporated through the reduced gravity.

For stability analysis, we assume the zonal wave solution of the linear perturbation equations of the form

$$\left\{ \begin{array}{c} u \\ v \\ h \end{array} \right\} = \mathrm{Re} \left\{ \begin{array}{c} U(y) \\ iV(y) \\ H(y) \end{array} \right\} e^{ik(x-ct)} \tag{3}$$

where k is the wavenumber, c is the complex phase speed and capital letters denote the complex wave amplitudes. Substituting Eq. (3) in Eqs. (1a)–(1c), we obtain the following equations:

$$\{(\bar{u} - c)k - iK\}U - (f - \bar{u}_y)V + g^*kH = 0 \tag{4a}$$

$$\{(\bar{u} - c)k - iK\}V + fU + g^*H_y = 0 \tag{4b}$$

$$(\bar{u} - c)kH + (H_0 + \bar{h})(kU + V_y) + \bar{h}_yV = 0. \tag{4c}$$

Kuo (1978) has pointed out that for a barotropic instability problem of zonal flow in a channel, it is more convenient to solve the equation in V than in U or H. He outlined

a procedure for obtaining the V equation which can be written as

$$V_{yy} + [\{f\bar{u} + \bar{u}_y(2\sigma - iK^*)\}/\Delta - 2f\bar{u}/c_g^2]V_y +$$
$$+ [[\beta - \bar{u}_{yy} - ff^*\sigma/c_g^2 + f^*\{f\bar{u} + \bar{u}_y(2\sigma - iK^*)\}/\Delta]/(\sigma - iK^*) -$$
$$-(\beta\bar{u} + f\bar{u}_y - [k^2\Delta + f\bar{u}\{f\bar{u} + \bar{u}_y(2\sigma - iK^*)\}/\Delta]/c_g^2)]V = 0 \qquad (5)$$

where

$$f^* = f - \bar{u}_y; \quad K^* = K/k; \quad \sigma = \bar{u} - c; \quad c_g^2 = g^*(\bar{h} + H_0); \quad \Delta = c_g^2 - \sigma(\sigma - iK^*). \qquad (6)$$

To find the solution of Eq. (5), the necessary lateral boundary conditions are obtained by assuming that the wave motions are confined between two vertical walls separated by a distance D in the meridional direction, which implies that

$$V = 0 \text{ at } y = 0 \text{ and } y = D. \qquad (7)$$

H is computed from the following equation, which is obtained after eliminating U between Eqs. (4a) and (4c):

$$H = \{g^*(H_0 + \bar{h})f^* - f\bar{u}(\sigma - iK^*)\}V +$$
$$+ g^*(H_0 + \bar{h})(\sigma - iK^*)V_y/kg^*\{g^*(H_0 + \bar{h}) - \sigma(\sigma - iK^*)\}. \qquad (8)$$

Using the computed values of V and H, U is computed from Eq. (4a).

3. ENERGY EQUATIONS

The zonal average wave kinetic energy per unit mass, K_w, and the zonally and vertically averaged wave potential energy per unit mass, P_w are given by

$$K_w = (UU^* + VV^*)/4 \qquad P_w = H\Phi^*/\{4(H_0 + \bar{h})\} \qquad (9)$$

where Φ is the complex geopotential amplitude of the wave and the asterisk denotes the complex conjugate of the quantity in this section only.

We note the following relations for unstable waves:

$$(K_w)_t = kc_i(UU^* + VV^*)/2 \qquad (P_w)_t = kc_iH\Phi^*/[2(H_0 + \bar{h})] \qquad (10)$$

where c_i is the imaginary part of c.

The kinetic energy equation is easily obtained by first multiplying Eqs. (4a) and (4b) by $-U^*$ and V^*, respectively, then adding and separating the imaginary part from the final equation, we get

$$kc_i(UU^* + VV^*)/2 = -\{K(UU^* + VV^*) + \bar{u}_y\,\text{Im}(VU^*) + \text{Im}(k\Phi U^* - \Phi_y V^*)\}/2 \qquad (11)$$

The first term on the right of Eq. (11) represents the kinetic energy dissipation due to friction and the second term represents the barotropic kinetic energy conversion from the basic state to the wave. The conversion term also includes the contribution from the wave energy transport. The expression $\text{Im}(VU^*)/2$ in the second term represents the zonal average momentum transport by the wave in the meridional direction. The last term denotes the work done by the pressure gradient force.

Similarly, the potential energy equation is obtained from Eq. (4c) as follows

$$\bar{h}_y \, \text{Im}(V\Phi^*)/\{2(H_0 + \bar{h})\} + \text{Im}(V\Phi^*)_y/2 - \text{Im}(kU^*\Phi - V^*\Phi_y)/2. \tag{12}$$

We notice that the last terms of Eqs. (11) and (12) are the same but occur with opposite sign. Therefore, we can say that the work done by the pressure gradient force represents the conversion from potential to kinetic energy.

4. NUMERICAL METHOD

The numerical solutions (eigenvalues and eigenfunctions) of Eq. (5) for a given wavenumber k are obtained by an iterative scheme, which starts with a first guess value $c^{(1)}$ for c. A set of 15 first guess values of c is considered for the calculations. For obtaining the first guess values, the semicircle theorem given by Howard (1961) is used, this states that for two-dimensional inviscid disturbances in a non-rotating system, all values of c lie in an upper semicircle of radius $(U_{max} - U_{min})/2$, centred at $(U_{max} + U_{min})/2$, where U_{max} and U_{min} are the maximum and the minimum values of $\bar{u}(y)$.

$$c_j^{(1)} = \tfrac{1}{2}\{(U_{max} + U_{min}) + (U_{max} - U_{min}) \, e^{ij\pi/15}\} \tag{13}$$

where $j = 1, 2, \ldots, 15$. We integrate Eq. (5) for each $c_j^{(1)}$ from the boundary point $y = 0$ as a simple numerical marching problem to determine V up to $y = D$. For this purpose, we use the fourth-order Runge–Kutta method. We specify $V_y = 1/\Delta y$ at $y = 0$, where Δy is the grid interval along the y axis, as the additional boundary condition required by the numerical method. In general the nth iterative solution $V^{(n)}$ will not satisfy the boundary condition at $y = D$. In order to determine the correction to c_n, we assume that the value of $V^{(n)}$ at $y = D$ is G, a continuous function of c in the neighbourhood of c_n. We modify c_n by δc, so that the boundary condition is satisfied at $y = D$. Then we have

$$G(c_n + \delta c) = G_0 + G'\delta c + G''\delta c^2/2 + \ldots = 0 \tag{14}$$

where the prime denotes differentiation with respect to c. The derivatives are evaluated at $c = c_n$ by using the centred finite differencing scheme. δc is taken as the smaller absolute value of the roots of the following quadratic equation, as suggested by Kuo (1978):

$$G_0/(\delta c)^2 + G'/\delta c + G''/2 = 0. \tag{15}$$

Eigenvalues were also computed for the initial guess values obtained from Pedlosky's semicircle theorem for the three-dimensional quasi-geostrophic waves on a beta plane (1964). The eigenvalues so computed were found to be identical to the values obtained for the initial guess given by Eq. (13). Further, it was noted that more than one initial value converged to the same final value and more than one unstable mode was found for the given k. The mode with maximum positive c_i for given k was selected as the most unstable mode.

5. MODEL PARAMETERS

For the stability analysis in this study, we choose the zonal flow at 700 mb because the onset vortex appeared initially as a closed cyclonic circulation at this level as has been mentioned earlier. Further, the influence of boundary layer friction on the motion at 700 mb is expected to be significantly less than the motion at 850 mb. The zonal flow

winds at 700 mb for the period 10–14 June 1979 on a 2·5°×5° latitude–longitude grid over the region 10°S to 20°N 40°E to 80°E are obtained from objectively analysed streamlines and isotachs (Krishnamurti *et al.* 1979). The longitudinally averaged zonal wind profile is constructed for each day and also for the 5-day mean flow (10–14 June). Figure 1 shows the wind profiles on 10, 12, 14 June and the 5-day mean profile. Hereafter these profiles are referred as UJ0, UJ2, UJ4 and UA profiles, respectively. UJ0, UJ2 and UJ4 profiles are representative of flows prior to the formation of the onset vortex, its first appearance as a closed cyclonic circulation at 700 mb and the formation of the onset vortex at 850 mb, respectively. Grid point values at 1° intervals are obtained by fitting each observed profile to a half-cosine Fourier series.

The basic zonal wind $\bar{u}$ profiles clearly exhibit a progressive strengthening of westerly flow over the Arabian Sea (Fig. 1). This leads to a gradual strengthening of the barotropic instability, as can be inferred from the computed $\bar{q}$ (absolute vorticity profiles (Fig. 2)).

We consider the lower and upper layers of the two-layer system as the 1000–600 mb and 600–200 mb layers, respectively, for computing g^*. The computed value of g^* is $0.776 \, m s^{-2}$ and the mean constant height of the lower layer is chosen as 4 km. For terminating the iterative process, 10^{-6} has been prescribed as an upper limit to the convergence error. It is noticed that not more than 25 iterations are required for the convergence of the iterative procedure. f_0 and β are evaluated at the middle of the channel (5°N).
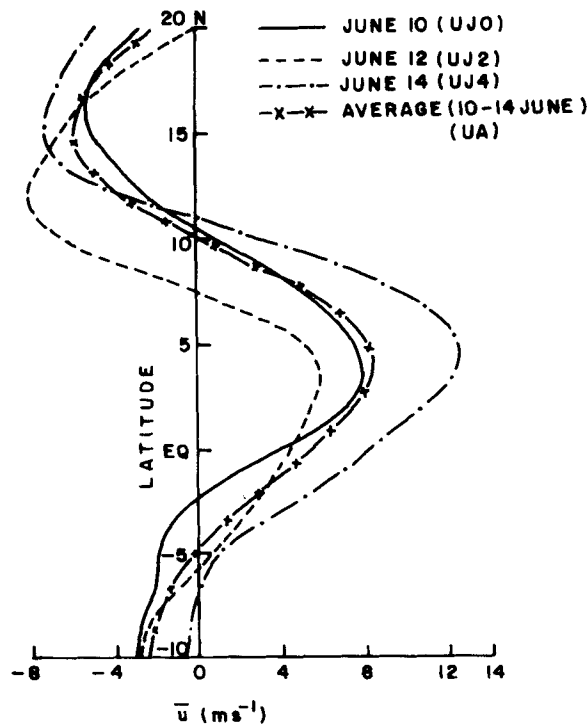

Figure 1.   Meridional profiles of longitudinally averaged (40°E–80°E) zonal wind for 10, 12, 14 June and the 5-day mean (10–14 June) profiles.
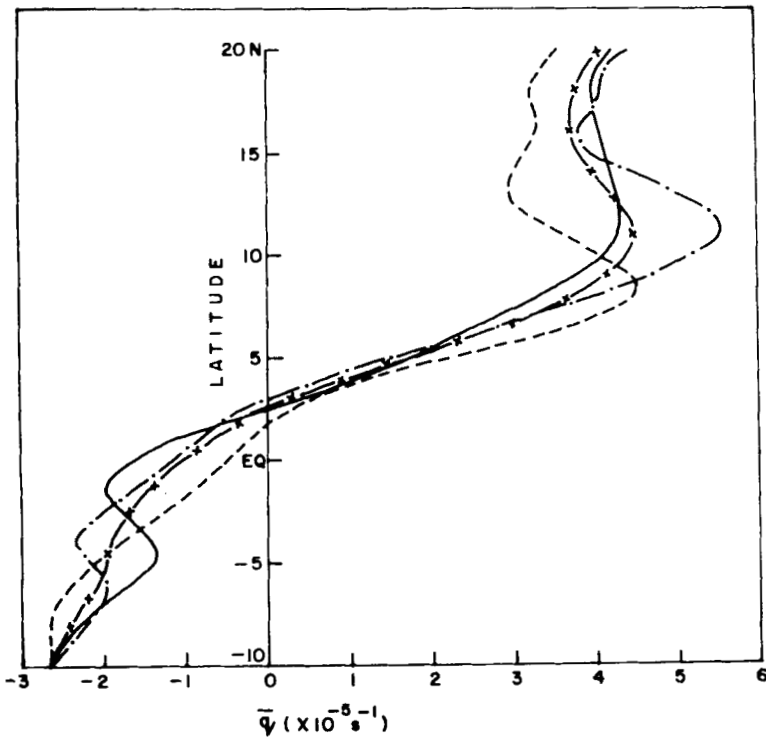
Figure 2. Meridional profiles of absolute vorticity for UJ0, UJ2, UJ4 and UA profiles.

6. RESULTS

Numerical solutions of the eigenvalue problem are obtained for the latitudinal grid interval of 2° in the wavelength range 1000–4500 km at intervals of 250 km. A few numerical solutions were also obtained at the higher resolution of 1°. Comparison between the low and high resolution solutions indicates that the 2°-latitude interval is an adequate resolution for this study.

(a) Growth rate and phase speed

Growth rate curves as a function of wavelength are computed for each individual day basic flow profile. Figure 3(a) illustrates the inviscid primitive equation growth rate curve only for UJ0, UJ2 and UJ4 and UA profiles because these are considered to be adequate for the purpose of evaluating the importance of barotropic instability in the initial formation of the monsoon onset vortex. Phase speed variation with wavelength is presented in Fig. 3(b). The pre-onset basic flow on the 10th is weakly unstable, with growth rates less than $0.1 \, \text{day}^{-1}$, and after two days, i.e. on the 12th, the flow abruptly becomes strongly unstable with a maximum growth rate of $0.33 \, \text{day}^{-1}$.

Thus, the basic flow at 700 mb has evolved rather quickly to a state where the vortex can form via a barotropic instability mechanism and can subsequently grow by the barotropic process. This evolution of barotropic instability has also been noted by Krishnamurti *et al.* (1981) and Mak and Kao (1982) for the basic flow at 850 mb for the same period in their non-divergent barotropic and linear balance barotropic–baroclinic
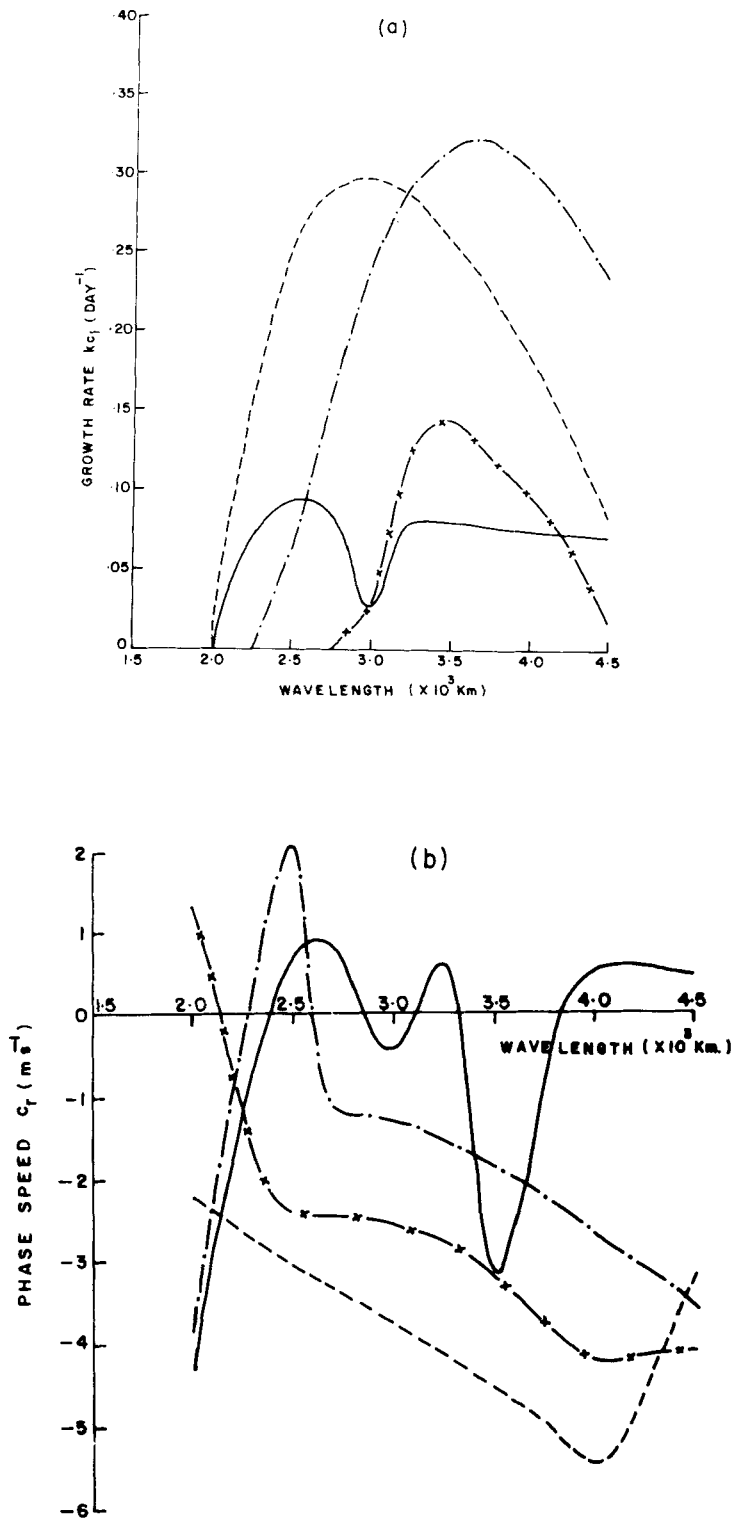
Figure 3. Spectra of (a) growth rate and (b) phase speed for UJ0, UJ2, UJ4 and UA profiles for the primitive equation case.

instability analyses, respectively. The preferred wavelength varies monotonically with time, starting at 2500 km on the 10th and attaining 3500 km on the 14th. The observations also confirmed the progressive increase in the horizontal scale of the onset vortex, particularly on 14–15 (Huj 1980). It is not suggested here that the observed variation in the horizontal scale of the onset vortex during its formative stage is due to the variation in the preferred scale of the unstable mode, because it is difficult for an unstable mode with an e-folding time of several days to adjust its structure so rapidly.

The preferred wavelength for the 14 June profile has an e-folding time of $3 \cdot 1$ days, a wavelength of 3500 km and a phase speed of $1 \cdot 9 \, \text{m s}^{-1}$. The averaged preferred wavelength during the period 10–14 June obtained from the preferred wavelengths on individual days is in good agreement with the observed wavelength of the onset vortex as estimated by Krishnamurti et al. (1981).

The primitive equation barotropic unstable waves possess divergence and are non-geostrophic. In order to isolate non-geostrophic effects on growth rates, the growth rate and phase velocity spectra are computed for non-divergent and divergent cases and are presented in Figs. 4(a) and (b) and in Figs. 5(a) and (b), respectively. In the divergent case the divergence effect is included in the quasi-geostrophic barotropic vorticity equation through the $R_0^{-2} \, \partial \phi / \partial t$ term (Lipps 1963), where R_0 is the Rossby radius of deformation and has a value 1000 km for lower tropospheric disturbances in the tropics. The primitive equation growth rates are slightly less than those of non-divergent values but almost equal to the divergent values. This leads to the conclusion that the stabilization of the flow due to the non-geostrophic effects is mainly contributed by the divergence. This conclusion does not rule out the possibly significant contributions of non-geostrophic effects other than divergence in determining the structure of primitive equation unstable modes.

The growth rate and phase speed spectra and the structure were also computed for viscous primitive equation modes with the Rayleigh (drag) coefficient K as $10^{-6} \, \text{s}^{-1}$ (not presented). A comparison between the viscous and inviscid cases has indicated that there is no significant effect on the unstable modes except for a decrease in growth rates.

(b) *Structure of the unstable wave*

Geopotential and horizontal wind vector fields associated with the most unstable primitive equation modes for UJ2 and UJ4 profiles are presented in Figs. 6(a) and (b), respectively. In these figures, the geopotential values are arbitrarily normalized to a maximum value of 10 and the wind vectors are normalized so that the maximum wind speed is equal to the grid size. In all figures one wavelength (L) in the x direction is shown. The geopotential low and high are marked by L and H, respectively, whereas the centres of cyclonic and anticyclonic circulation are shown by C and A, respectively. The symbols D and $-D$ indicate the location of divergence and convergence maxima, respectively. y_c indicates the critical or steering latitude where $c_r = \bar{u}$.

An examination of the wave structures has revealed that the cyclonic circulation centre lies about 3° to the south of the geopotential low, a similar feature, but with a larger separation between the two, is seen in the balance unstable modes (Mak and Kao 1982). The cyclonic centre for the 14 June basic flow is quite close to the observed cyclonic circulation centre at 9°N. Further, the cyclonic centre is moved northward by 2° during the period 12–14 June. The wave tilt becomes more pronounced with the passage of time. Further, the tilts of the unstable waves are more pronounced than the observed tilt.

It is seen from the wave structures that the motions are very close to the geostrophic
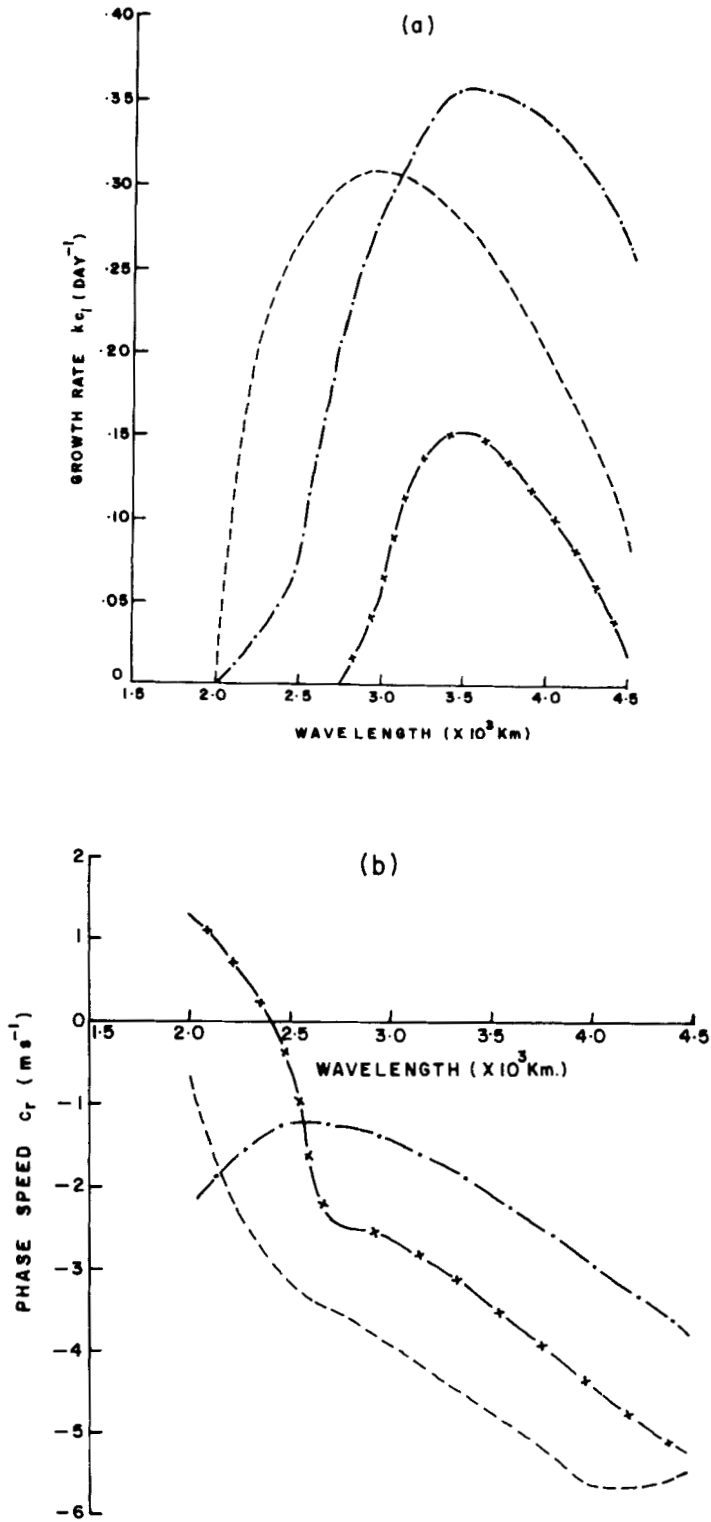
Figure 4. Spectra of (a) growth rate and (b) phase speed for UJ2, UJ4 and UA profiles for non-divergent case.
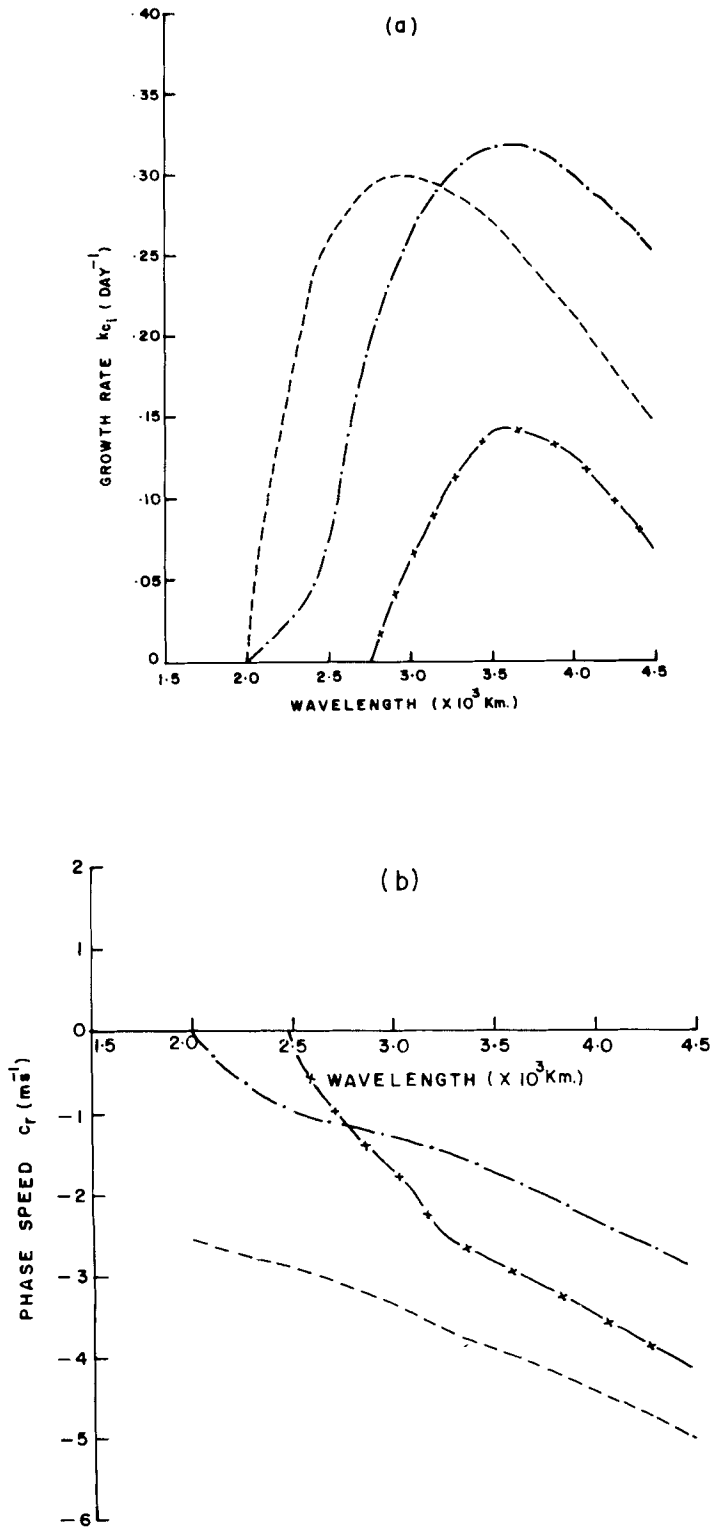
Figure 5.   Spectra of (a) growth rate and (b) phase speed for UJ2, UJ4 and UA profiles for the divergent case with the Rossby radius of deformation value as 1000 km.
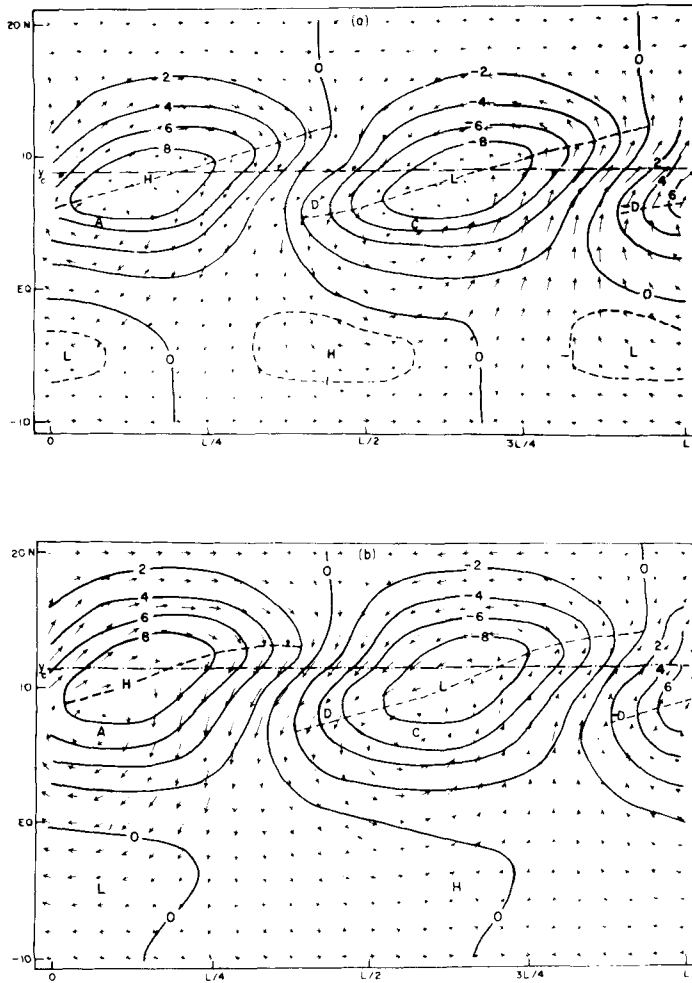
Figure 6. Geopotential and horizontal wind vector fields (in arbitrary units) in the horizontal plane for primitive equation preferred wave for (a) UJ2 and (b) UJ4 profiles. Contour separation, 2 arbitrary units.

only north of 10°N. The horizontal wind convergence is located to the east of the cyclonic vorticity centre, which induces an eastward propagation because $\bar{q} > 0$ in the region q being the absolute vorticity. This physical process is absent in the non-divergent model. This explains why the westward phase speeds of primitive equation modes are less than those of non-divergent modes.

We present in Figs. 7(a) and (b) the geopotential amplitude and phase angle profiles of the primitive equation and divergent unstable modes for the UJ4 profile. Significant differences in the meridional scales, the locations of amplitude maximum and the latitudinal tilts are noticed between the two cases. We can conclude that the ageostrophic effects play an important role in determining the structure of unstable modes.

For a realistic comparison of the unstable wave with the observed onset vortex, the distribution of geopotential and the wind vector fields after superposing the normalized
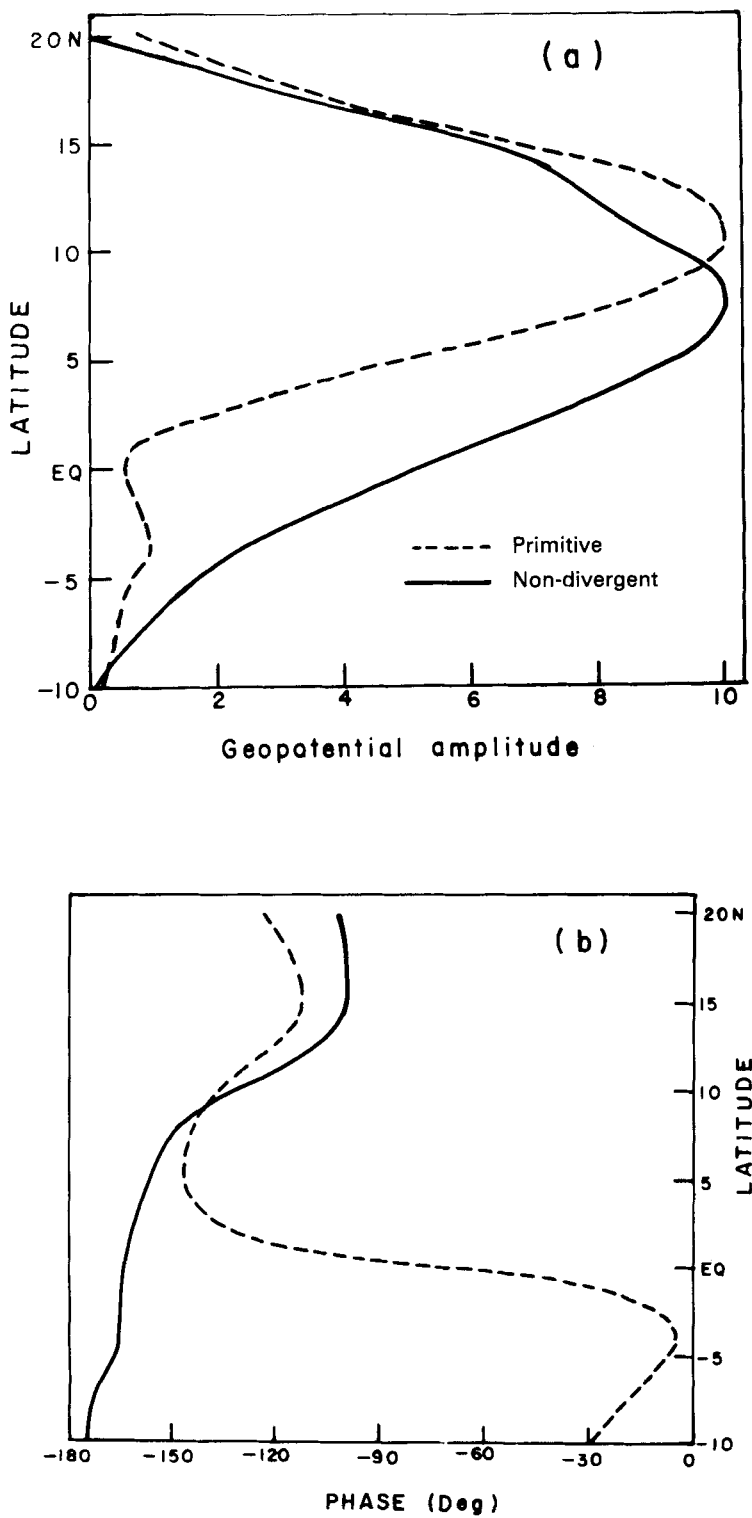
Figure 7.   Geopotential (a) amplitude (in arbitrary units) and (b) phase angle profiles for the non-divergent
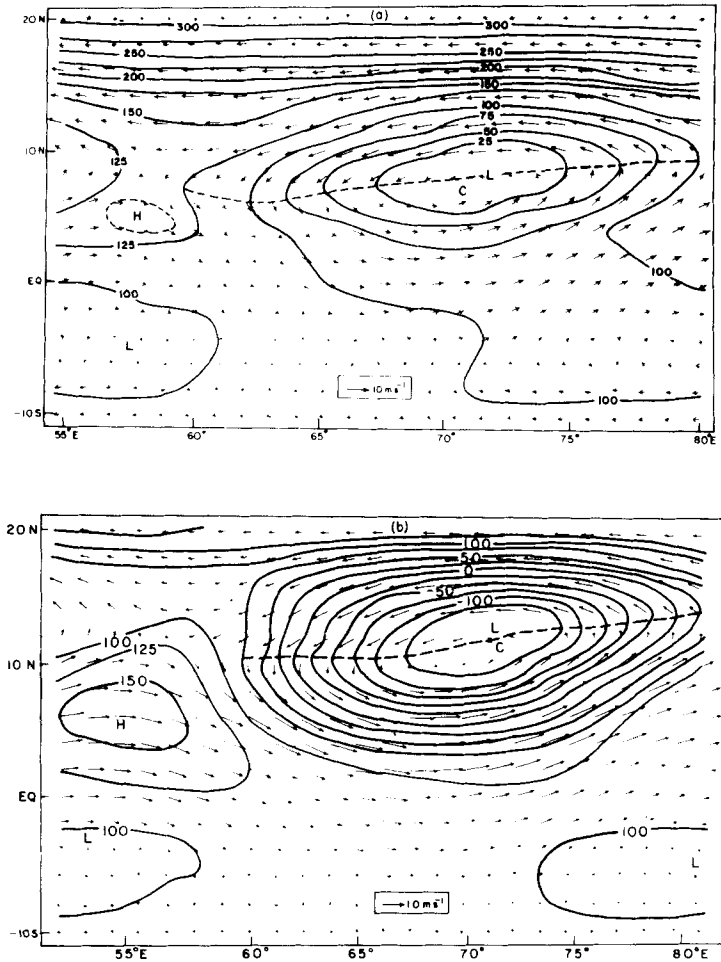(continuous) and primitive equation (dashed) preferred waves for UJ4 profiles.

Figure 8. The total geopotential and the normalized horizontal wind vector fields superposed on the basic state of the primitive equation preferred wave at 700 mb for (a) UJ2 and (b) UJ4 profiles. Contour separation $25\,m^2s^{-2}$. The letters C and L refer to the cyclonic circulation centre and geopotential low, respectively. The geopotential trough axis is marked by a dashed line.

primitive equation wave on the basic state are obtained and are presented in Figs. 8(a) and (b), respectively. We have considered the departure of the basic state geopotential from the constant depth of the lower layer and also have normalized waves for the 12 June and 14 June to the maximum meridional winds of $4\,m\,s^{-1}$ and $6\,m\,s^{-1}$, respectively. These values correspond to the observed maximum departure of the meridional wind from its longitudinal average in the region 40°E–80°E 10°S–20°N for 12 June and 14 June, respectively. Due to the superposition, the wave geopotential low area is contracted in the meridional direction and is elongated in the zonal direction to such an extent that it attains a very prominent appearance in the map. Further, the tilt of the geopotential trough axis is less pronounced than the tilt as seen from the wave fields alone. In the total fields, the cyclonic circulation centre nearly coincides with the low centre. The overall agreement of the total field rather than the wave field alone is closer to the observed vortex.

(c)   *Zonal propagation of unstable waves*

We consider the linear primitive equation barotropic vorticity equation

$$\zeta_t + \bar{u}\zeta_x + v\bar{q}_y + \bar{q}(u_x + v_y) = 0 \tag{16}$$

where ζ is the relative vorticity of the perturbation. To the south of y_c, the zonal advection of cyclonic wave vorticity is eastward except very close to y_c, where it is westward. It has been earlier mentioned that the distribution of divergence with respect to the vorticity is such that it leads to the eastward motion of the wave. Equation (16) implies that the westward propagation of the wave to the south of y_c is entirely due to the meridional transport of $\bar{q}$. In this connection, it is noted that $\bar{q}_y > 0$ to the south of y_c and $v > 0$ to the west of the cyclonic circulation centre and $v < 0$ to its east. The maximum northerly wind is located at a distance of about $L/4$ to the west of the cyclonic circulation centre. This implies that cyclonic vorticity is generated by the meridional advection of $\bar{q}$ to the west of y_c, which induces the westward movement to the wave. It is clear that to the north of y_c the westward propagation to the wave is mainly due to the zonal advection of ζ.

(d)   *Momentum transports*

The zonal average momentum transports $\overline{u'v'}$ produced by the normalized primitive equation preferred modes for UJ2 and UJ4 wind profiles are computed and are shown in Fig. 9. A comparison of the momentum transport profiles with their corresponding $\bar{q}$ profiles indicates that the maximum northward transport of westerly momentum takes place at the latitude where $\bar{q}$ maximum is located.
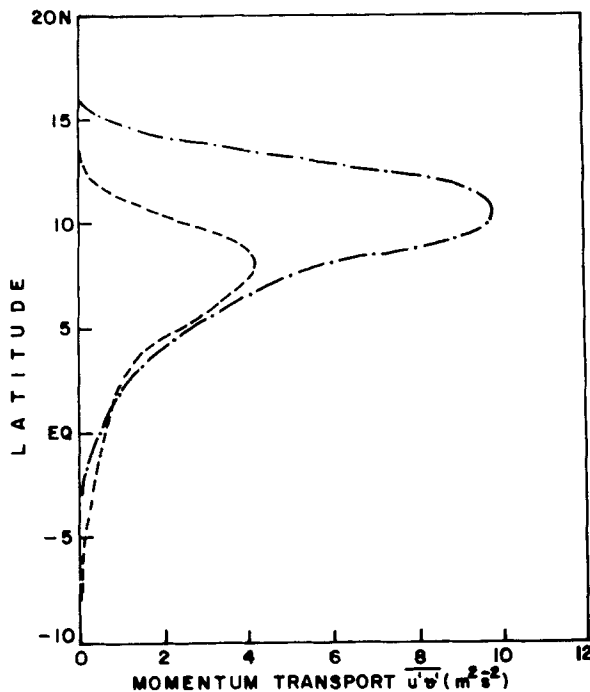

Figure 9.   Meridional profiles of zonally averaged momentum transports $\overline{u'v'}$ for UJ2 and UJ4 profiles.

In many diagnostic studies of tropical disturbances, the barotropic energy conversion as a possible energy source for their maintenance is generally inferred from the tilt of the trough line, assuming that the disturbances are quasi-geostrophic. Gruber (1974) has shown for divergent flow, that it is possible for a streamline pattern with trough and ridges oriented SW–NE to have zonally averaged angular momentum transports associated with it which are directed southward.

The quasi-geostrophic average momentum transport $\overline{(u'v')}_{QG}$ is given by (Kuo 1949)

$$\overline{(u'v')}_{QG} = k/(2f_0^2)\,|\Phi^2|\,d\alpha/dy \tag{17}$$

where $d\alpha/dy$ denotes the meridional slope of the wave trough line. The $d\alpha/dy$ profile is shown in Fig. 10. It can be inferred by using Eq. (17) that the quasi-geostrophic momentum transports are southward in the belt 4°S to 6°N, while the transports associated with the primitive equation wave are northward in this region (Fig. 9). Thus, it is quite possible that the direction of momentum transports, as inferred from the wave tilt based on the quasi-geostrophic assumption, may not be in agreement with the observed transports in the equatorial region. This may lead to erroneous conclusions regarding the energy source for tropical disturbances.
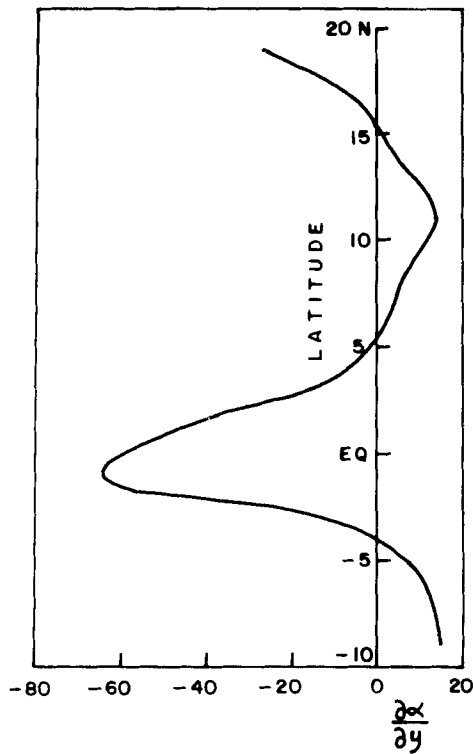

Figure 10.   Meridional slope (in arbitrary units) of the trough line for the primitive equation wave.

(e)   *Energetics of the preferred wave*

The computed meridional profiles of K_w and P_w, and $C(K_b, K_w)$ and W_p of the normalized primitive equation preferred wave for UJ4 are presented in Figs. 11(a) and (b), respectively. An examination of the profiles indicates that the wave energy maxima and their sources are located at the same latitude, which is close to $\bar{q}$ maxima. It is concluded that K_b to K_w conversion dominates in the domain average.

7.   CONCLUSION

It has been concluded from the results that barotropic instability is one possible mechanism for the initial formation of the onset vortex. Inclusion of the divergence effect in the simple form in the quasi-geostrophic vorticity equation enables account to be taken of the non-geostrophic effect on growth rates and the preferred wavelengths. The non-geostrophic effects play an important role in determining the horizontal structure of the unstable modes. The primitive equation unstable mode is found to be in better agreement with the observed structure of the onset vortex than the quasi-geostrophic mode.

It has been seen that the total basic state and the normalized primitive equation unstable wave velocity and geopotential fields have some features which are closer to the observed vortex than those appearing in the fields associated with the wave alone.

Meridional advection of the basic state absolute vorticity by the wave has been identified as the only physical process responsible for the westward propagation of the wave to the south of the critical latitude; while to the north of it, it is the zonal advection of the wave relative vorticity by the basic zonal wind. In the equatorial region the northward directed momentum transports are associated with the SE–NW tilted wave trough. These transports are in opposite directions to those implied by the quasi-geostrophic assumption. Therefore, it is quite possible that an erroneous conclusion regarding the source of energy for the vortex may be arrived at if we examine its latitudinal tilt alone in the equatorial region.

It is well known that linear instability theory alone is not adequate to explain why the observed vortex is cyclonic rather than anticyclonic. However, it is seen that in the total field only a cyclonic vortex is present, this is due to the fact that the unstable wave develops in the region of cyclonic shear of the basic zonal flow which strengthens the cyclonic circulation and weakens the anticyclonic circulation of the wave. This provides an explanation of why the observed vortex is cyclonic rather than anticyclonic. The present study provides no explanation for the preferred longitude of vortex formation and is not able to account fully for the observed northward component of its movement. It is expected that the inclusion of basic state meridional flow in a stability analysis will be able to provide answers to these questions.
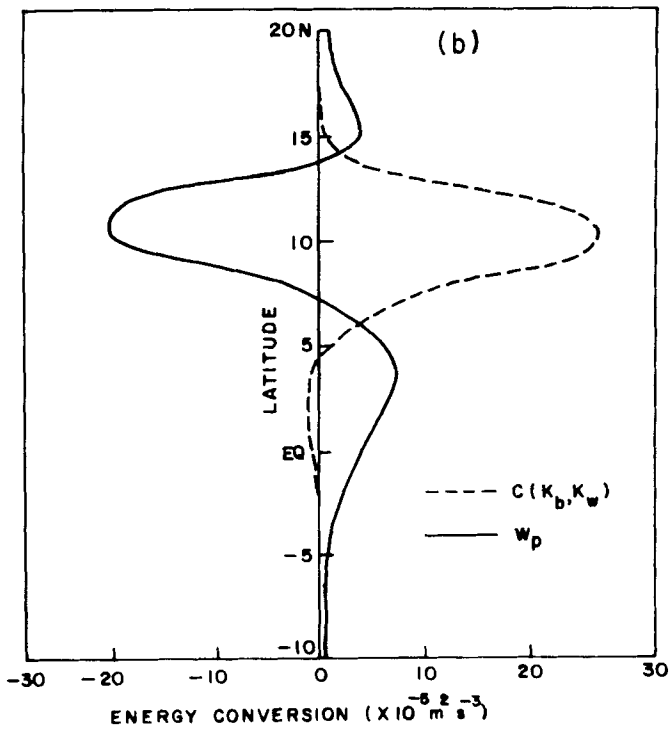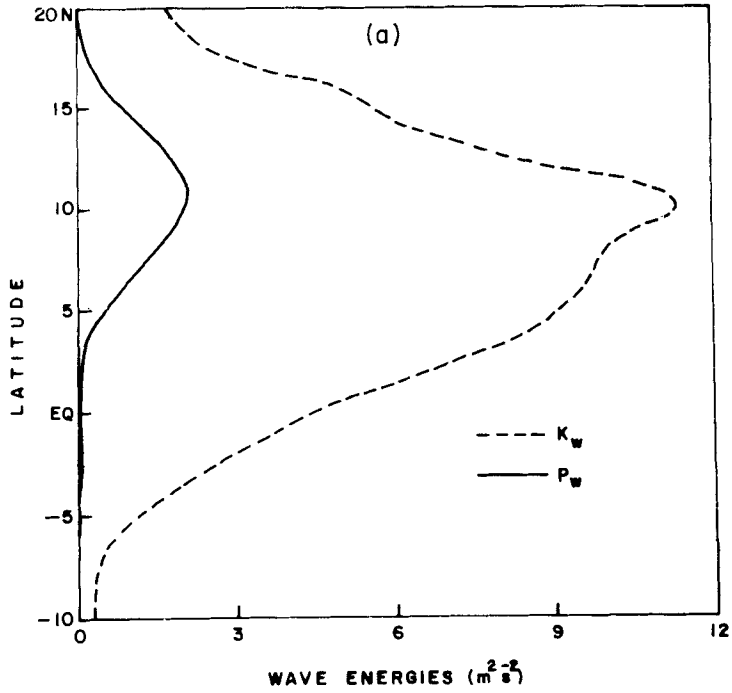
Figure 11.   Meridional profiles of (a) wave kinetic energy K_w and wave potential energy P_w associated with the normalized primitive equation preferred wave and (b) meridional profiles of the barotropic energy conversion $C(K_b, K_w)$ and work done by the pressure gradient force W_p.

REFERENCES

Ananthakrishnan, R., Srinivasan, V., Ramakrishnan, A. R. and Jambunathan, R.   1968   'Synoptic features associated with onset of southwest monsoon over Kerala', in *Forecasting Manual. FMU Rept. No. IV*-18.2., India Met. Dept., Poona-5, India

Borde, R. W. and Man-Kin Mak   1978   On the mechanism of monsoonal mid-tropospheric cyclone formation. *J. Atmos. Sci.*, **35**, 1473–1484

Gruber, A.   1974   On stream line patterns and momentum transports. *J. Atmos. Sci.*, **31**, 1161–1163

Howard, L. N.   1961   Note on a paper of John W. Miles. *J. Fluid Mech.*, **10**, 509–512

Huj, D. Y.   1980   'A case study of the formation and structure of a monsoon depression over the Arabian sea', in *FGGE Operation Report*, 9: *Results of summer MONEX field phase research (part A)*. WMO Publication, Geneva, 92–113

Krishnamurti, T. N., Ardanuy, P., Ramanathan, Y. and Pasch, R.   1979   'Quick-look summer MONEX atlas, Part II. The onset phase', Florida State University Report No. 79–5., Tallahassee, Florida, U.S.A.

Krishnamurti, T. N., Ardanuy, P., Ramanathan, Y. and Pasch, R.   1981   On the onset vortex of the summer monsoon. *Mon. Wea. Rev.*, **109**, 344–363

Kuo, H. L.   1949   Dynamic instability of two-dimensional non-divergent flow in a barotropic atmosphere, *J. Meteor.*, **6**, 105–122

  1978   A two-layer model study of the combined barotropic and baroclinic instability in the tropics. *J. Atmos. Sci.*, **35**, 1840–1860

Lipps, F. B.   1963   Stability of jets in a divergent barotropic fluid. *ibid.*, **20**, 120–129

Mak, M. K.   1975   The monsoonal mid-tropospheric cyclogenesis. *ibid.*, **32**, 2246–2253

Mak, M. K. and Kao, C.-Y. J.   1982   An instability study of the onset vortex of the southwest monsoon 1979. *Tellus*, **34**, 358–368

Mishra, S. K. and Salvekar, P. S.   1980   Role of baroclinic instability in the development of monsoon disturbances. *J. Atmos. Sci.*, **37**, 383–394

Mukherjee, A. K. and Paul, D. K.   1980   'Influence of Arabian sea cyclone systems on the onset of monsoon'. in *FGGE Operation Report*, 9, *Results of summer MONEX field phase research (part A)*, WMO Publication, Geneva, 62–67

Pedlosky, J.   1964   The stability of currents in the atmosphere and the oceans: Part I. *J. Atmos. Sci.*, **21**, 201–219